Autonomous Trail Following

Masoud Hoveidar-Sefid and Michael Jenkin
Electrical Engineering and Computer Science Department and York Centre for Field Robotics,
Lassonde School of Engineering, York University, Toronto, Canada

Keywords: Autonomous Navigation, Trail Following, Path Finding.

Abstract: Following off-road trails is somewhat more complex than following man-made roads. Trails are unstructured and typically lack standard markers that characterize roadways. Nevertheless, trails can provide an effective set of pathways for off-road navigation. Here we approach the problem of trail following by identifying trail-like regions; that is regions that are locally planar, contiguous with the robot's current plane and which appear similar to the region in front of the robot. A multi-dimensional representation of the trail ahead is obtained by fusing information from an omnidirectional camera and a 3D LIDAR. A k-means clustering approach is taken based on this multi-dimensional signal to identify and follow off-road trails. This information is then used to compute appropriate steering commands for vehicle motion. Results are presented for over 1500 frames of video and laser scans of trails.

1 INTRODUCTION

Trail following is a hard problem in comparison with the well known autonomous road following which is aided by many detectable and well known features available in highways and streets. As is the case for the road following algorithm, the goal of the trail following algorithm is to process sensor data so as to produce motion commands that drive the robot along the trail and centre the robot on it. Any trail following algorithm is informed by the data of the sensors that are connected to the robot. More sensors provide an advantage for more robust sensing and hence a more robust algorithm. The work presented here relies on the fusion of vision and LIDAR information and then segmenting the fused datasets using a k-means clustering algorithm into 'trail' and 'non-trail' regions based on the assumption that the robot is currently on the trail, and that the region directly in front of the robot is "trail-like". Based on this clustering process, a motion command is constructed to drive the robot along the trail and to centre the robot on it.

2 PREVIOUS WORK

There is a large road following literature associated both with 'off-road' roads as well as hard surface roadway following. Previous work on path finding and following task can be classified based on the sensors employed in three different categories: visual approaches, laser approaches and integrated vision-laser approaches.

Vision-based Approaches: Vision-based following approaches can be traced back to the 1980's (e.g., (Waxman et al., 1985),(Kuan et al., 1988) and (Liou and Jain, 1987)), and research in this field continues to today. It is not practical to review all approaches here (see (DeSouza and Kak, 2002), (Bar Hillel et al., 2014) and (Buehler et al., 2007) for reviews), but rather a few examples are used to illustrate the vast number of different approaches. (Moghadam et al., 2010), present a self-supervised learning algorithm for terrain classification that exploits near-field stereo vision in front of the robot and combines this information with terrain features extracted from monocular vision. (Moghadam and Dong, 2012) use an alternative approach for road direction estimation, based on the vanishing point of the road. The algorithm first localizes the vanishing point based on one image frame and then uses a sequence of images to predict the direction of the given road.

Laser-based Approaches: The main advantages of using a LIDAR sensor are that they provide a 3D representation of the environment and operate independently of the lighting conditions. The major disadvantages of LIDAR sensors are their lack of dense resolution and their need to emit energy into the enviornment. Many LIDAR sensors are able to return

Hoveidar-Sefid, M. and Jenkin, M.
Autonomous Trail Following.
DOI: 10.5220/0006468404250430
In *Proceedings of the 14th International Conference on Informatics in Control, Automation and Robotics (ICINCO 2017) - Volume 2*, pages 425-430
ISBN: Not Available

the intensity of the points as well which can be exploited when detecting different suface features independently from the lightning (see (von Reyher et al., 2005), (Kammel and Pitzer, 2008) and (Ogawa and Takagi, 2006)). As an example, (Kammel and Pitzer, 2008) used LIDAR intensity values to detect the lane markings due to their cue difference from the background (i.e., road) and to extract the curb's position on the road based on the height change in the laser range finder data. (Hernández and Marcotegui, 2009) and (Cremean and Murray, 2006) used LIDAR to detect the curbes and consequently the edges of the road ahead. Single beam LIDAR sensors are only able to detect obstacles and features in the plane of the laser beam. Multiple 2D LIDAR sensors or 3D laser scanners, detect more features of the environment. An improved road detection and following scheme (see (Kammel and Pitzer, 2008) and (Thrun et al., 2006), for example) can be achieved using multiple LIDAR scanners in comparison to the single 2D LIDAR approach (see (von Reyher et al., 2005) and (Zhang, 2010), for example).

Integrated Vision-laser-based Approaches: The integration of more sensors can enhance environmental perception. Fusing both visual information and laser range information enables a robot to have a more robust perception of the surrounding environment and the trail within it. (Rasmussen, 2002) describes an approach with a laser range finder and camera for the road following task, using four different features; height and smoothness of the points in front of the robot and color and texture features obtained from an on-board camera. Rasmussen used a neural network to classify different kinds of roads (paved or unpaved) using data sets of images and laser information from similar road scenarios. In the DARPA Grand Challenge in 2005 (DARPA, 2016), the Stanley robot, which won the competition, used a combination of vision and laser range finder for task of road detection in off-roads and desert terrains (Thrun et al., 2006). Equipped with five 2D laser range finders, Stanley was able to classify the terrain to three different classes; obstacle, drivable and unknown. An obstacle is defined on a grid cell around the robot which two nearby points of data have a height difference of more than a defined vertical distance threshold. Using this map of the road, Stanley computed a quadrilateral in front of the robot containing all possible drivable grid cells and used this region to perform color classification of the further road ahead to increase the range of road detection. Stanley could maintain high speeds in navigation and was able to handle the sudden changes in the surface type of the road as well.

Although there have been considerable successes in the navigation of roadways by autonomous systems, such algorithms are not necessarily well suited for trail following as trails typically lack the formal structure of roadways. Here we consider the problem of following trails which are characterized by providing a continuous ground plane upon which to travel and a visual and structure appearance that is different from the surrounding environment and consistent with the view in front of the robot.

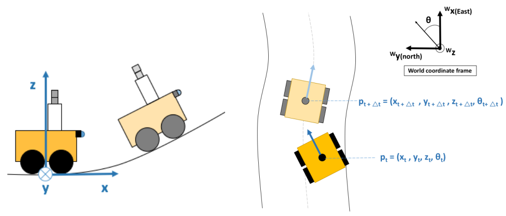

(a) (b)

Figure 1: Coordinate frames. (a) shows the robot coordinate frame placed underneath the center of mass of the robot on the ground plane at point $p = (x, y, z)$. (b) shows a bird's eye view of the robot on the path in two subsequent frames at time t and $t + \Delta t$ with its position and orientation in the world coordinate frame.

3 PROBLEM DEFINITION

For trail following, it is assumed that the robot is on the trail at time t, and the goal is to obtain the local twist vector (V, ω) that moves the robot along the trail while centering the robot on it. so that the robot has moved along the trail and is (more) centered on it at time t+1. Specifically, it is assumed that

- The robot is on the trail (p_t is on trail).
- The robot is more or less centered on the trail and looking along the trail.
- The path on the trail is more or less flat (i.e., the trail is drivable by the robot).
- The trail is characterized by sensor features which differentiate it from the surroundings.

The robot combines visual and range information from the local environment and labels the region around the robot as either trail or non-trail based on the assumptions above. The goal of the algorithm is to (i) detect that there exists a drivable trail in front of the robot (the assumptions above are met), and if so (ii) to characterize the trail and to estimate the twist vector that will cause the robot to move forward along the trail and center itself on it (see Fig. 1).

4 TRAIL FOLLOWING

The basic approach followed here is to construct a hyper-dimensional image that characterizes both deviation from the ground plane and per pixel image information, and then assuming that the robot is currently on the trail to utilize the k-means clustering algorithm on a reduced dimensional version of this image to identify trail versus non-trail locations. This information is then used to construct a local motion command (twist vector) that will drive the robot along the trail and keep the robot centered on it. An overview of the approach is shown in Fig. 2.

The algorithm utilizes both wide field visual and LIDAR data. Data is obtained from a Velodyne HDL-32E 3D laser scanner (velodyne, 2016) that obtains a 360 degree view of the space and a forward-facing Kodak Pixpro SP360 camera (kodak, 2016) mounted on the front of the robot.

4.1 Processing The Laser Data

Many methods have been used to extract different features of point cloud datasets. Prior knowledge about the characteristic of the plane can help in extracting a more accurate plane model. Robust algorithms such as RANdom SAmpling Consensus (RANSAC) (Fischler and Bolles, 1981) and M-estimator SAmpling Consesus (MSAC) (Torr and Zisserman, 2000) have been used successfully to extract plane information from laser data. Here we exploit the fact that we are interested in grouping data points that correspond to the ground plane that is currently supporting the vehicle. That is, planes that pass near $p = (0,0,0)$ and that have a normal near $\hat{n} = (0,0,1)$. A simplified version of the MSAC plane fitting algorithm (Algorithm 1) is used to find the plane that best fits the laser dataset while grouping laser points into inlier and outlier groups. Triplets of points (p_1, p_2, p_3) are repeatedly extracted from the point cloud and used to form a plane that is consistent with $\hat{n} = (0,0,1)$. Then each point in the dataset is tested against this plane. Points are identified as either inliers or outliers based on the distance from the point to the plane. A cost fit function is computed as the sum of the distances from the plane for inliers plus the cutoff distance for outliers. This score function is then used to select the 'best fit' plane and to identify the inlier/outlier sets. As shown in Fig. 2, laser data is first clipped to the region in front of the robot. The resulting data is then used within the MSAC plane fitting algorithm to determine a cost function that represents the deviation from the robot ground plane for each laser reading. This cost function is then mapped into the camera image and the two signals integrated.

Algorithm 1: M-estimator SAmpling Consensus algorithm (Torr and Zisserman, 2000) for plane fitting.

Input $(P[x,y,z], \theta_{th}, \hat{n}_P, N_{trials}, \delta)$
for $a = 1 : N_{trials}$ **do**
  for non-colinear random points $p_1, p_2, p_3 \in P[x,y,z]$ **do**
    if $cos^{-1}(\hat{n}_{S_a} \cdot \hat{n}_P) < \theta_{th}$ **then**
      remove p_1, p_2, p_3 **from** $P[x,y,z]$
      for all $[x_i, y_i, z_i] \in P[x,y,z]$ **do**
        $e_i = |distance(S_a, [x_i, y_i, z_i])|$
        if $e_i \leq \delta$ **then**
          $\rho(e_i) = e_i$
          add $\{[x_i, y_i, z_i]\}$ to $P_a^{inliers}$
        else
          $\rho(e_i) = \delta$
          add $\{[x_i, y_i, z_i]\}$ to $P_a^{outliers}$
        $C_a = \sum_i \rho(e_i)$
$k = argmin_j\{C_j\}$
return C_k, $P_k^{inliers}$, $P_k^{outliers}$

4.2 Processing the Visual Data

In order to integrate the visual data with the data from the LIDAR, the camera must be calibrated. A mathematical model of omnidirectional cameras and a calibration method using a planar checkerboard target are described in (Micusik and Pajdla, 2003) and (Scaramuzza et al., 2006) respectively. Let X_i be a 3D point in world coordinates. Then let $u'' = [u'', v'']^T$ be the projection of X_i on the sensor plane and $u' = [u', v']^T$ is the projection of point u'' on camera plane. u' and u'' are related to each other by an affine transformation due to miss-alignment of the camera and sensor plane axes and digitizing process of light rays to pixels. u'' can be described as $u'' = Au' + t$, where $A \in \Re^{2\times2}$ and $t \in \Re^{2\times1}$. Define a projection function g, relating a u'' point on the sensor plane to a vector pointing out of the camera origin O to the corresponding 3D point X_i. The resulting camera model is given by $\lambda.g(u'') = \lambda.g(Au' + t) = PX_i$, $\lambda > 0$. This treats $X_i \in \Re^4$ as a homogeneous point $[x,y,z,1]^T$, $P \in \Re^{3\times4}$ as a perspective transformation matrix and λ is the normalized distance to X_i. In order to calibrate the camera, A and t matrices and the function g should be estimated. Using this estimation we can extract a vector pointing to the scene point from point O to every point X_i. g is a non-linear function and is defined as $g(u'', v'') = (u'', v'', f(u'', v''))^T$, where f is a rotationally symmetric function with respect to the axis of the sensor. Function f is modeled as $f(u'', v'') = a_0 + a_1\rho + a_2\rho^2 + ... + a_n\rho^n$, where the model parameters are a_i, $i = 0, 1, 2, ..., n$ and n is the degree of the polynomial. ρ is the Euclidean dis-

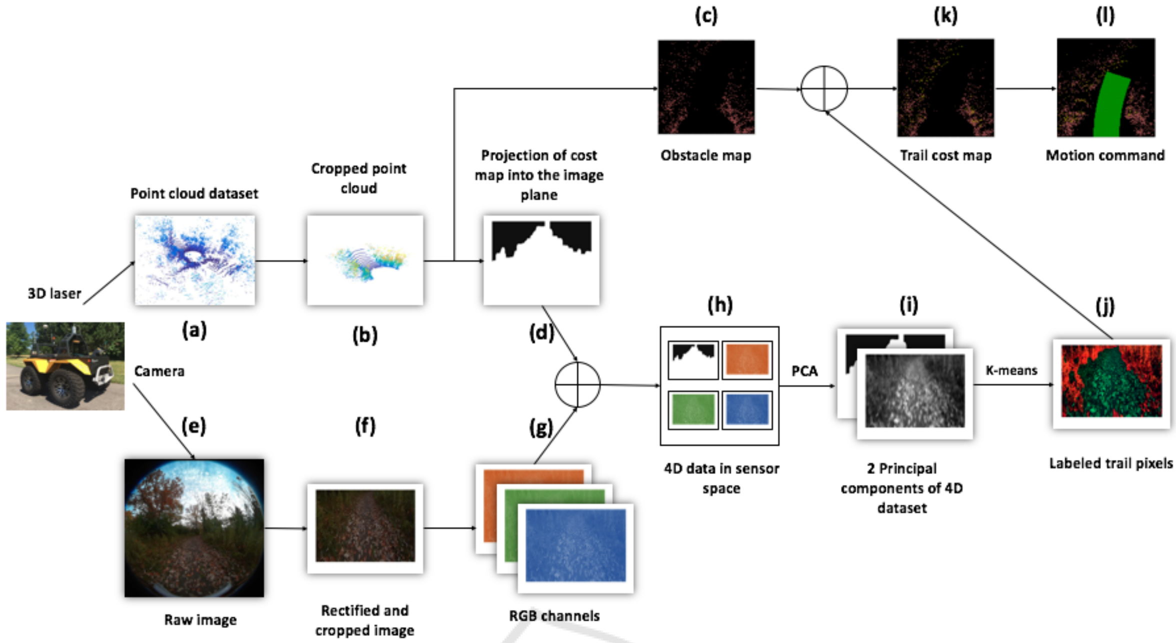

Figure 2: Data from the two sesnors are processed into a common reference frame. Laser data is recoded as error relative to the expected ground plane. When integrated with the camera signal this produces a 4D sensor signal (r,g,b,e) which then goes through a PCA process to obtain a 2D signal for segmentation. The k-means clustering algorithm is used to segment regions similar to the region directly in front of the robot (which is assumed to be trail) from other regions.

tance of point (u'', v'') from sensor's geometric center, hence $\rho = \sqrt{u''^2 + v''^2}$. The completed approach to estimate these parameters is presented in more details in (Scaramuzza et al., 2006). Calibration parameters are used to define the relation between any 3D point in the world coordinate and the pixel on the image plane.

4.3 Merging Vision and Laser

In order to integrate the data of camera and laser into a single measurement vector, a common reference frame is required. When integrated with the output of the vision sensor this obtains a 4DOF signal (r, g, b, e) where e is the remapped C_k cost from the best plane fitting function obtained from the laser data.

There is not necessarily a correspondence point in point cloud dataset for every pixel in the image; for this reason it is necessary to assign each obstacle point $P[x_i, y_i, z_i]$ to a group of pixels ${}^{(u_c,v_c)}G$ instead, where (u_c, v_c) is the position of the correspondence pixel of the reprojection of point $X_i[x_i, y_i, z_i]$ on the image plane. This pixel group is created by dilating the pixel (u_c, v_c).

Recognizing the redundant nature of this 4D signal and the cost associated with performing clustering on high dimensional data, the dataset is then compressed using principal component analysis (PCA) [Abdi and Williams, 2010]. This allows the 4DOF signal to be represented with a lower dimensional signal thus reducing the cost of the clustering algorithm.

4.4 Trail Following

In order to label pixels of an image to different groups, k-means clustering (MacQueen et al., 1967) is used. After applying this algorithm, the dataset is divided into a defined number of clusters, where each cluster is represented with a centroid and indexes of each data entry belonging to that cluster. The k-means clustering algorithm with a fixed number of k clusters and a d dimensional dataset with n number of entities can be solved in the order of $O(n^{dk+1})$ (see (Inaba et al., 1994)). After identifying the k clusters, each cluster is represented by its mean μ_k and covariance matrix Σ_k and is assigned to one of the two categories: *trail*, or *non-trail*. An immediate region in front of the robot is assumed to contain all the characteristics of the drivable trail. This region is called Region of Interest on the Trail or ROIT. ROIT is selected as a rectangle in the camera reference frame and is modeled using a Mixture of Gaussian (MOG) distributions. Pixels of ROIT are defined as g number of Gaussians with mean of μ_i and covariance of $\Sigma_i; \{i = 1, 2..., g\}$. Cluster k is counted as trail if it similar to one of the g Gaussians in ROIT. This similarity is determined through the Mahalanobis distance as $d(i, j) = (\mu_i - \mu_j)^T (\Sigma_i + \Sigma_j)^{-1} (\mu_i - \mu_j)$ where $\{i =$

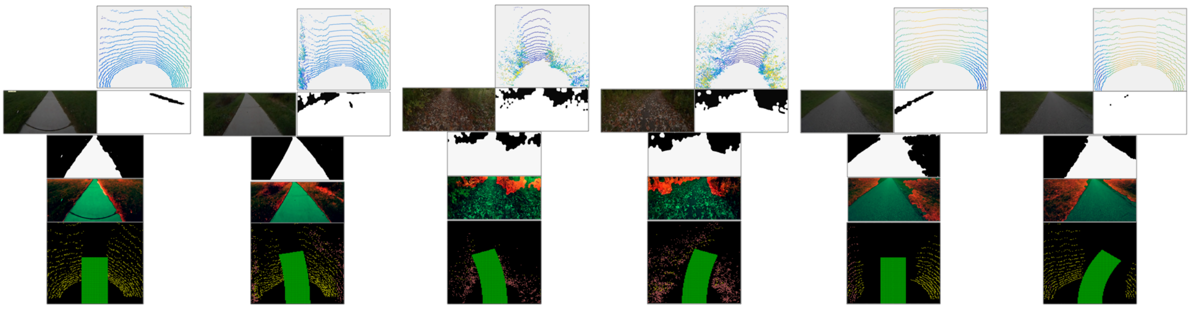

(a) (b) (c) (d) (e) (f)

Figure 3: Results of the trail following algorithm on different sample trails. The point cloud data, obstacle mask in the image plane along with the trail image, segmented mask of the drivable and non-drivable path on the trail with a green and red visualization of the outputs and the predicted trajectory of the robot after the computed motion command are depicted sequentially for every frame. (a, b) show two frames from the concrete dataset, (c, d) are two selected frames from the dirt trail and (e, f) show the results for the algorithm on an asphalt trail.

$1, 2..., g\}$ and $\{j = 1, 2..., k\}$. μ and Σ are the mean and covariance matrices of each Gaussian distribution, respectively. $d(i, j)$ denotes the Mahalanobis distance between the two distributions. For every cluster, if $d(i, j)$ is less than a threshold, the cluster is considered to be similar and it is labeled as trail, otherwise it is identified as being different and the cluster represents a non-trail region. The results of this assignment is shown in Fig. 2(j).

To update the 2D cost map (obtained with point clouds) shown in Fig. 2(c) with the results of the clustering algorithm (shown in Fig. 2(j)), each grid cell in the 2D cost map that is assumed to be free space is checked against the label of its corresponding pixel. If the corresponding pixel of a grid cell labeled as non-road, then the cost will be updated to the value of $\frac{c_{max}+c_{min}}{2}$, where c_{max} is the highest cost (denoting the existence of an obstacle) and c_{min} represent a free space.

Different rotational velocities coupled with a common forward motion velocity are considered, and the trajectory with the minimum cost over a small temporal window is chosen.

5 EXPERIMENTAL RESULTS

Three different datasets have been recorded using the on-board Kodak Pixpro SP360 camera and a Velodyne HDL- 32E 3D laser scanner from the trails of the campus of York University. These datasets were captured on three different trail types: 1) a concrete trail surrounded by grass and trees, 2) a dirt trail covered with leaves and 3) a pedestrian asphalt trail surrounded with grass. Results of the algorithm on three trail types are shown in Fig. 3.

In order to asses the accuracy of the trail following algorithm, a set of 1500 natural images from the three datasets were used. These images were hand labeled by two human observers who were asked to label the drivable path in each frame and these labeled images were used as ground truth. A binary mask of these labeled images is used to evaluate the accuracy of the output of the algorithm. The labeled output of the algorithm is also extracted as a binary mask. Using a pixel-wise XNOR function on the ground truth mask and output of the algorithm, by dividing the number of pixels with the value of 1 ($N_{\text{XNOR-pixels}}$) to the total number of the pixels in the image ($N_{\text{all-pixels}}$), accuracy of the algorithm on each frame is calculated as $(N_{\text{XNOR-pixels}}/N_{\text{all-pixels}}) \times 100\%$.

Fig. 4 shows histograms of the calculated for each of the three trail types. The overall accuracy of the algorithm on the dirt dataset, asphalt dataset and concrete dataset is 60.85%, 86.3% and 96.8% respectively.

6 CONCLUSION

In this paper we presented an adaptive trail following algorithm for autonomous robot navigation on different types of trails, using visual information of the environment, point cloud data obtained from the onboard sensors. Finally, the output of the algorithm on a diverse set of trail types were presented with successfully detected trail and non-trail regions along with a motion command to move the robot forward in the environment.

ACKNOWLEDGMENTS

The support of NSERC Canada and the NSERC Canadian Field Robotics Network (NCFRN) are gratefully acknowledged. We would also like to thank

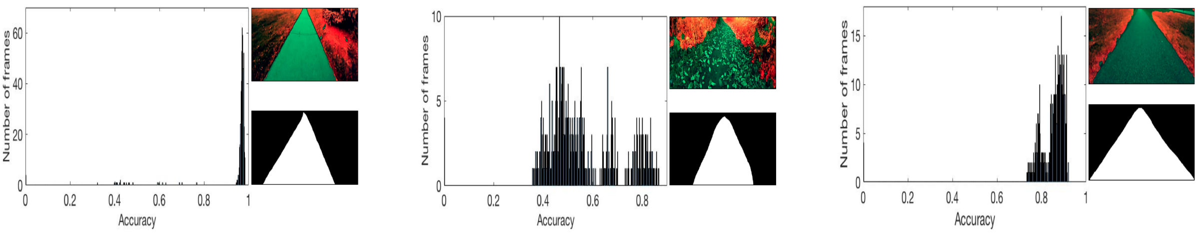

(a) Concrete (b) Dirt (c) Asphalt

Figure 4: The accumulative accuracy histogram charts along side their corresponding frame with highest accuracy and its hand labeled ground truth mask of (a) concrete, (b) dirt and (c) asphalt datasets respectively. These histograms show the distribution of the frames based on their computed accuracy in comparison to the ground truth dataset.

Emmanuel Mati-Amorim and Arjun Kaura who hand labeled the test datasets.

REFERENCES

Bar Hillel, A., Lerner, R., Levi, D., and Raz, G. (2014). Recent progress in road and lane detection: a survey. *Machine Vision and Applications*, pages 1–19.

Buehler, M., Iagnemma, K., and Singh, S. (2007). *The 2005 DARPA Grand Challenge: The Great Robot Race*, volume 36. Springer Science & Business Media.

Cremean, L. B. and Murray, R. M. (2006). Model-based estimation of off-highway road geometry using single-axis ladar and inertial sensing. In *Proc. ICRA 2006.*, pages 1661–1666.

DARPA (2016). The Defense Advanced Research Projects Agency (DARPA) website.

DeSouza, G. N. and Kak, A. C. (2002). Vision for mobile robot navigation: A survey. *IEEE PAMI*, 24(2):237–267.

Fischler, M. A. and Bolles, R. C. (1981). Random sample consensus: a paradigm for model fitting with applications to image analysis and automated cartography. *Comm. ACM*, 24(6):381–395.

Hernández, J. and Marcotegui, B. (2009). Filtering of artifacts and pavement segmentation from mobile lidar data. In *ISPRS Workshop Laserscanning 2009*.

Inaba, M., Katoh, N., and Imai, H. (1994). Applications of weighted voronoi diagrams and randomization to variance-based k-clustering. In *Proc. 10th Ann. Symp. Comp. Geom.*, pages 332–339.

Kammel, S. and Pitzer, B. (2008). Lidar-based lane marker detection and mapping. In *2008 IEEE Intell. Vehic. Symp.*, pages 1137–1142.

kodak (2016). The Kodak camera website.

Kuan, D., Phipps, G., and Hsueh, A. C. (1988). Autonomous robotic vehicle road following. *IEEE PAMI*, 10(5):648–658.

Liou, S.-P. and Jain, R. C. (1987). Road following using vanishing points. *Computer Vision, Graphics, and Image Processing*, 39(1):116–130.

MacQueen, J. et al. (1967). Some methods for classification and analysis of multivariate observations. In *Proc. 5th Berkeley Symp. on Math. Stats. and Prob.*, volume 1, pages 281–297. Oakland, CA, USA.

Micusik, B. and Pajdla, T. (2003). Estimation of omnidirectional camera model from epipolar geometry. In *IEEE CVPR*, volume 1, pages I–485.

Moghadam, P. and Dong, J. F. (2012). Road direction detection based on vanishing-point tracking. In *IEEE/RSJ IROS*, pages 1553–1560.

Moghadam, P., Wijesoma, W. S., and Moratuwage, M. (2010). Towards a fully-autonomous vision-based vehicle navigation system in outdoor environments. In *ICARCV*, pages 597–602.

Ogawa, T. and Takagi, K. (2006). Lane recognition using on-vehicle lidar. In *IEEE Int. Vehic. Symp.*, pages 540–545.

Rasmussen, C. (2002). Combining laser range, color, and texture cues for autonomous road following. In *IEEE ICRA*, volume 4, pages 4320–4325.

Scaramuzza, D., Martinelli, A., and Siegwart, R. (2006). A flexible technique for accurate omnidirectional camera calibration and structure from motion. In *IEEE ICVS*, pages 45–45.

Thrun, S., Montemerlo, M., Dahlkamp, H., Stavens, D., Aron, A., Diebel, J., Fong, P., Gale, J., Halpenny, M., Hoffmann, G., et al. (2006). Stanley: The robot that won the darpa grand challenge. *J. Field Robot.*, 23(9):661–692.

Torr, P. H. and Zisserman, A. (2000). Mlesac: A new robust estimator with application to estimating image geometry. *CVIU*, 78(1):138–156.

velodyne (2016). The Velodyne 3D Lidar website.

von Reyher, A., Joos, A., and Winner, H. (2005). A lidar-based approach for near range lane detection. In *IEEE Intel. Vehic. Symp.*, pages 147–152.

Waxman, A., Moigne, J., and Srinivasan, B. (1985). Visual navigation of roadways. In *IEEE ICRA*, volume 2, pages 862–867.

Zhang, W. (2010). Lidar-based road and road-edge detection. In *IEEE Int. Vehic. Symp.*, pages 845–848.